IOP Conf. Series: Materials Science and Engineering **307** (2018) 012079 doi:10.1088/1757-899X/307/1/012079

Effect of aluminum contents on sputter deposited CrAlN thin films

A Vyas[1, *], **Z F Zhou**[2] and **Y G Shen**[3]

[1]Department of Mechanical Engineering, The Hong Kong Polytechnic University, Hung Hom, Kowloon, Hong Kong, China
[2,3]Department of Mechanical and Biomedical Engineering, City University of Hong Kong, Kowloon, Hong Kong, China
[*]Email: mmavyas@polyu.edu.hk

Abstract. Pure CrN and CrAlN films with varied Al concentrations were prepared onto Si(100) substrates by an unbalanced reactive dc-magnetron sputtering system. The crystal structure, chemical states, and microstructure of the films were characterized by X-ray diffraction, X-ray photoelectron microscopy, transmission electron microscopy whereas mechanical properties were determined by nano-indentation measurements. XRD results showed a prominent (200) reflection in both CrN and CrAlN films. Results demonstrate that CrAlN films formed a solid solution and doping of Al atoms replace the Cr atoms affecting the lattice parameter and crystallization of the films. All Al doped films were of B1 NaCl-type structure, demonstrating that CrAlN films primarily crystallized in cubic structure. Microstructural investigation by TEM for a CrAlN film containing Al content of 24.1 at.%, revealed that there exists an amorphous/nanocrystalline domains (grains of about ~ 11 nm) and hardness increases 22% when compared with pure CrN film.

1. Introduction

Binary and ternary transition metal based nitride materials are applied in various industrial as well as engineering applications owing to their significant physical, chemical and mechanical properties including enhanced oxidation and corrosion resistance [1-3]. Nowadays, most metal formed or molded components are coated with chromium nitride (CrN) to improve the corrosion and oxidation resistance under severe environmental conditions [4-5]. However, due to limited hardness of CrN and its poor wear resistance, restricts its applications in the field of engineering such as machine parts, drills and cutting tools [6]. On the other hand, addition of Al, into CrN leads to the formation of a nanocomposite structure comprising of two phases, CrN/AlN, which helps in overcoming the issue of high temperature instability and gives higherhardness (>30 GPa) and enhanced anti-corrosion resistance, making chromium-aluminium-nitride (Cr-Al-N) films superior to CrN especially enhancing oxidation resistance at high temperatures. Microstructurally, formation of AlN phase at the CrN grain boundaries, helps suppress the oxidation in these high diffusive paths, and shields the enclosed two-phase CrN/AlN nanocomposite structure [7-9].

Up to now, nanocrystalline CrAlN composite films have been deposited by various techniques which include vacuum arc reactive deposition process, [10, 12], chemical vapor deposition (CVD) [13], and dc/rf reactive magnetron sputtering [14,15]. The crystal structure, microstructure, concentration, and corrosion resistance of these nanocomposite films have been studied in comparison with conventional binary nitrides of CrN and AlN films. However, due to lack of in-depth study on chemical bonding status and microstructure for sputter-deposited CrAlN films generates curiosity to investigate. In our

investigation, the effect of the small amount of Al added to CrN matrix on bonding status, microstructure and mechanical properties of CrAlN films is reported, in which new features which were not covered previously are presented here. X-ray photoelectron spectroscopy (XPS) was employed to investigate the chemical bonding status in the films. Phases in the films were revealed by X-ray diffraction (XRD). Nano-structural evolution was studied by employing high-resolution transmission electron microscopy (HRTEM) and transmission electron diffraction (TED). The mechanical properties were obtained by nanoindentation technique.

2. Experimental

CrN and CrAlN films with various Al contents were deposited onto Si(100) substrates using a close-field unbalanced dc-magnetron sputtering system (UDP650, Teer Coating Limited) with four high-purity targets (three Ti and one Al) in a mixture of Ar and N_2 gases. The substrates were ultrasonically cleaned in acetone then dried andplaced into the vacuum chamber. The base pressure in the chamber was 2×10^{-6} Torr, and the working pressure, was set at 1.5 mTorr. The Cr target current was set at 5 A and Al target current ranged from 0 to 10 A in order to acquire films with varied Al concentrations. The films deposited are namely, A0, A1, A2, A3, A4, A5, and A6. Film A0 is pure CrN and A6 with Al current of 10 A has the highest Al content of 24.1%. With target current ratio (I_{Al}/I_{Cr}) ranging from 0 to 2.0, the atomic ratio of Al/(Cr+Al) could be increased from 0 to 0.48 (in Table 1 in Section 3). The substrate rotation speed was 10 rpm. Films nominal thickness was 600 nm at a bias voltage of -80 V (250 kHz).

The crystal structure of the films was characterized by XRD using a Bragg-Brentano diffractometer (Simens D500). The elemental concentration and bonding status were investigated by XPS (PHI Quantum 2000) having monochromatic Al Kα X-ray source (hν=1486.6 eV) induced by 13 kV, 25 mA Al kα radiation. The nanostructure was analyzed by HRTEM (field emission JEOL 2010F) at 200 kV. Nanoindentation tests were repeated 8 times and depth was at <10% of the film thickness.

3. Results and discussion

The measured results for the films are shown in Table 1.

Table 1. The I_{Al}/I_{Cr} target current, elemental concentration, grain size, hardness, Young's Modulus and H/E ratio of sputter-deposited CrAlN films.

Sample	Target Current ratio (I_{Al}/I_{Cr})	Al content (at. %)	Al/(Cr+Al) ratio	N content (at. %)	Grain size *D* (nm)	H(GPa)	E(GPa)	H/E ratio
A0	0	0	0	47.5	11.8 ± 0.2	18.8 ± 0.7	225.0 ± 6.2	0.083
A1	0.2	2.3	0.04	48.4	11.5 ± 0.3	21.8 ± 1.0	233.2 ± 8.6	0.093
A2	0.4	6.3	0.12	49.8	11.3 ± 0.2	22.5 ± 1.3	242.1 ± 11.4	0.097
A3	0.8	12.8	0.25	48.7	11.4 ± 0.2	21.4 ± 1.3	233.0 ± 9.6	0.092
A4	1.2	17.1	0.33	49.2	11.1 ± 0.2	22.0 ± 1.2	233.5 ± 10.6	0.094
A5	1.6	21.5	0.43	50.3	10.7 ± 0.2	22.8 ± 1.2	238.0 ± 8.9	0.095
A6	2.0	24.1	0.48	49.2	10.8 ± 0.2	24.0 ± 0.9	255.0 ± 8.5	0.096

3.1 Crystal structure by XRD

The influence of Al doping on the lattice parameter of CrAlN films can be seen in Fig. 1. The inset of Fig. 1 shows the XRD patterns of CrAlN films (A0 to A6).

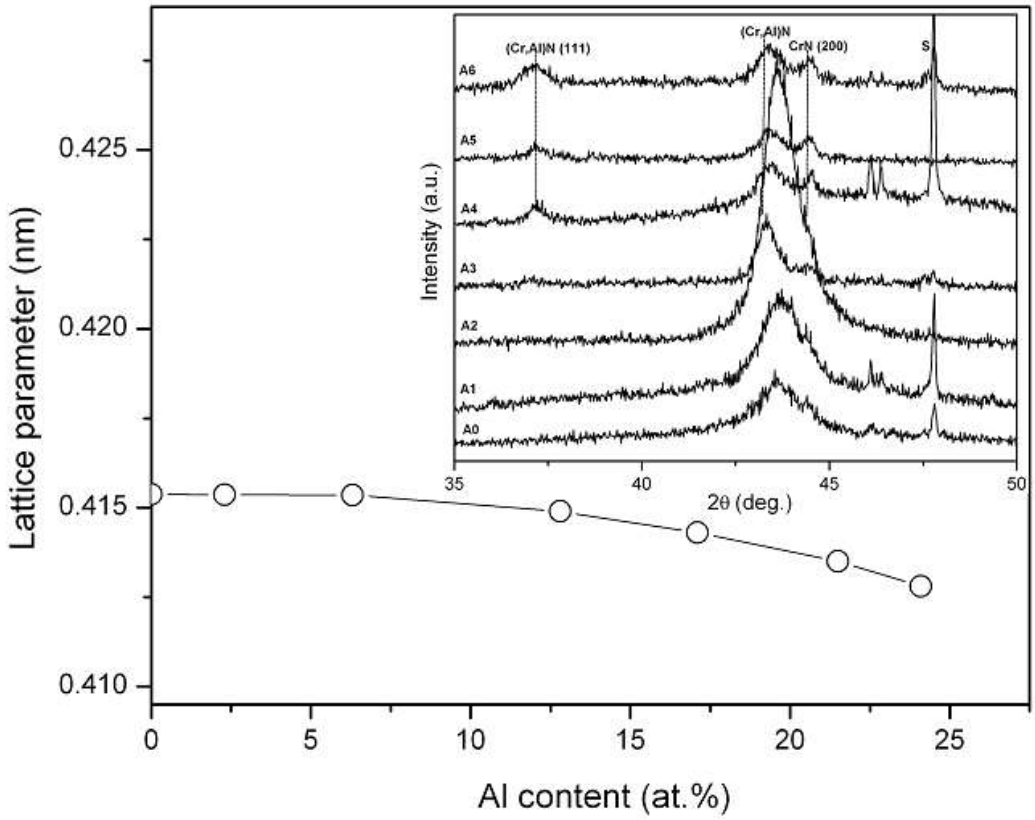

Figure 1. Dependence of lattice parameter in CrAlN films against Al content. Inset shows XRD patterns of pure CrN (A0) and CrAlN (A6) nanocomposite film with Al content of 24.1 at.% (S represents the substrate peak).

All deposited films exhibit polycrystalline structure. A B1-NaCl type cubic structure is observed in all the films [16-18]. Pure CrN film (A0), like all other films, prepared at substrate bias voltage -80V shows orientation of CrN (200) plane, which is a low intensity reflection. However, the broad peak indicates that the deposited film is not well crystallized at all and mostly amorphous at low substrate bias voltage, which is consistent with the previous report [19]. No other crystalline phase is identified in the XRD pattern of this film. In all our films, the orientation of the CrN (200) plane is due to the lowest surface energy of the crystal plane, similar to the results previously reported [20]. When the energy of incident ion bombardment increased during deposition, the CrN (200) plane was preferentially grown in order to reduce the surface energy [21]. The orientation (200) for A0 film, is identified at ~43.5^{o}, which is lower than the standard powder diffraction peak according to PCPDFWIN Version 2.3, JSPDF-ICDD (2002), suggesting occurrence of some stresses in the film. The diffracted (200) peaks obtained from film A3 with 12.8 at.% of Al content and film A6 with 24.1 at.% of Al are identified at ~43.6^{o} and ~43.7^{o}, respectively. It is noted that addition of Al results in enhanced crystallization, which is evidenced by the increase in CrN (200) peak intensities. It is also noted that a peak split occurs from film A3 onwards, resulting in a mixed peak consisting of (Cr,Al)N and CrN(200). Increasing Al content slightly shifts (200) peak towards a higher diffraction angle. Such a deviation towards a higher diffraction angle between the standard CrN (200) peak and that of CrAlN films is attributed to decrease of a lattice parameter in CrAlN films. The obvious gradual decrease in lattice parameter from 0.415 nm (A0 film) to 0.412 (A6 film) can be seen in Fig. 1, confirming the integration of Al atoms into cubic CrN lattice. The reason being,the covalent radius of Al (0.121 nm) is smaller as compared to Cr (0.139 nm) and makes possible to initiate the crystal lattice distortion (lattice contraction) which is in good agreement with previous studies [22, 23]. Also, when Al content is ≥ 17.1 at.%, the CrN (200) peak intensities are significantly decreased implying that crystallites in

the film became smaller and moreover, the CrN (111) peak with a weak intensity appears at ~37.2^{o}. At Al content of 24.1 at.%, the peak intensity of CrN (111) is found to increase. It has been reported [22] that since increasing Al substitution causes lattice distortion resulting in an increase in the film's strain energy, thus to combat the increase in the strain energy, a tendency of change of preferred orientation from (200) to (111) is seen. Moreover, for the film with Al content of 24.1 at.% (A6), there is no evidence of the presence of *w*-AlN (B4-Wurtzite type) structure [18].The reason is that there is a maximum solubility of cubic Al ~ 77 at.% in cubic CrN in order to see the crystal structure change from B1-NaCl to B4-wurtzite (which is AlN phase) [16-18]. Al contents in our films are much less than the maximum solubility limit. But such a change in crystal structure has been also reported [17, 18] at much lower Al content (58 at.%). In our case, the fact that the observed peak (200) broadening as well as splitting in the films is very prominent, suggesting probable phase formation of either *c*-AlN and *c*-CrN or combination of other (Cr,Al)N phases or sub-stoichiometric grain formation.

3.2 Chemical analysis by XPS and Microstructure evaluation by HRTEM analysis

Figure 2 shows Cr 2p, N 1s and Al 2p XPS core-level spectra of pure CrN (A0) and CrAlN (A6) films to illustrate the development of chemical states in the films due to Al addition. The metal Cr peak consists of two peaks originating from Cr 2p3/2 and Cr 2p1/2 bonding states. Fig. 3(a) is the deconvolution of the Cr 2p3/2 peak of A0 film, indicating the existence of two peaks centered at 575.0 eV representing a CrN phase whereas peak at 576.6 eV occurs because of the existence of Cr_2O_3. Peaks related to pure Cr at 574.3 eV and Cr_2N at 574.5 eV were not present [24]. The N 1s spectra of A0 film in Fig. 3(b), shows the existence of CrN peak at 396.8 eV and a weaker peak at 398.3 eV which can be related to surface oxidation [25]. The XPS core-level spectra of CrAlN film (A6, with al content of 24.1 at.%) are shown in Fig. 3(c). The peak related with Cr was centered at 575.0 eV originating from Cr 2p3/2. The deconvolution of Cr 2p3/2 peak showed that it contained three peaks positioned at 575.0 eV, representing a CrAlN phase, peak at 575.7 eV being a CrN phase and 577.5 eV representing a Cr_2O_3 phase, respectively. Metallic Cr and Cr_2N were once again not observed [24]. The Al 2p spectra in Fig. 3(d) showed characteristic peaks at binding energy 73.5 eV originating from CrAlN, whereas peak at 74.3 eV is from AlN and the peak at 77.6 eV represents Al_2O_3 phase. In Fig. 3(e) the deconvoluted spectra of N 1s showed a typical peak of CrN at 396.21 eV along with weaker peak at 397.4 eV that could be related to AlN [23, 26].

TEM observations were performed to determine the microstructural difference and phase formation of the films due to addition of Al. Figure 3 depicts the plane-view TEM images and the insets are corresponding selected area diffraction patterns (SAED) of pure CrN (A0) and CrAlN (A6) films. The inset in Fig. 3(a) shows diffused scattering, producing a continuous ring pattern indicating lack of significant crystallinity, which is in agreement with the XRD results. Basically, can be understood as, a microstructure that comprises of crystallinity and amorphous region that co-exists. A continuous ring is a consequence of the fine and small size of grain distribution whereas diffuse scattering is a consequence of mostly amorphous AlN_x region in the film. Fig. 3(b) shows a HRTEM image of CrAlN (A6) film with Al content of 24.1 at.%. The corresponding electron diffraction rings are shown in the inset. These diffraction rings show sharp diffraction spots in a circle typical for polycrystalline material. Moreover, the Cr(Al)N solid solution which is a nanocrystalline phase has already been seen in our XRD and XPS results. The amorphous phase AlN is marked by white circles in the TEM image. On comparing the two SAED inset images in Fig. 3, we can see that there is a marked difference between diffraction ring patterns of both CrN (A0) and CrAlN (A6) films.

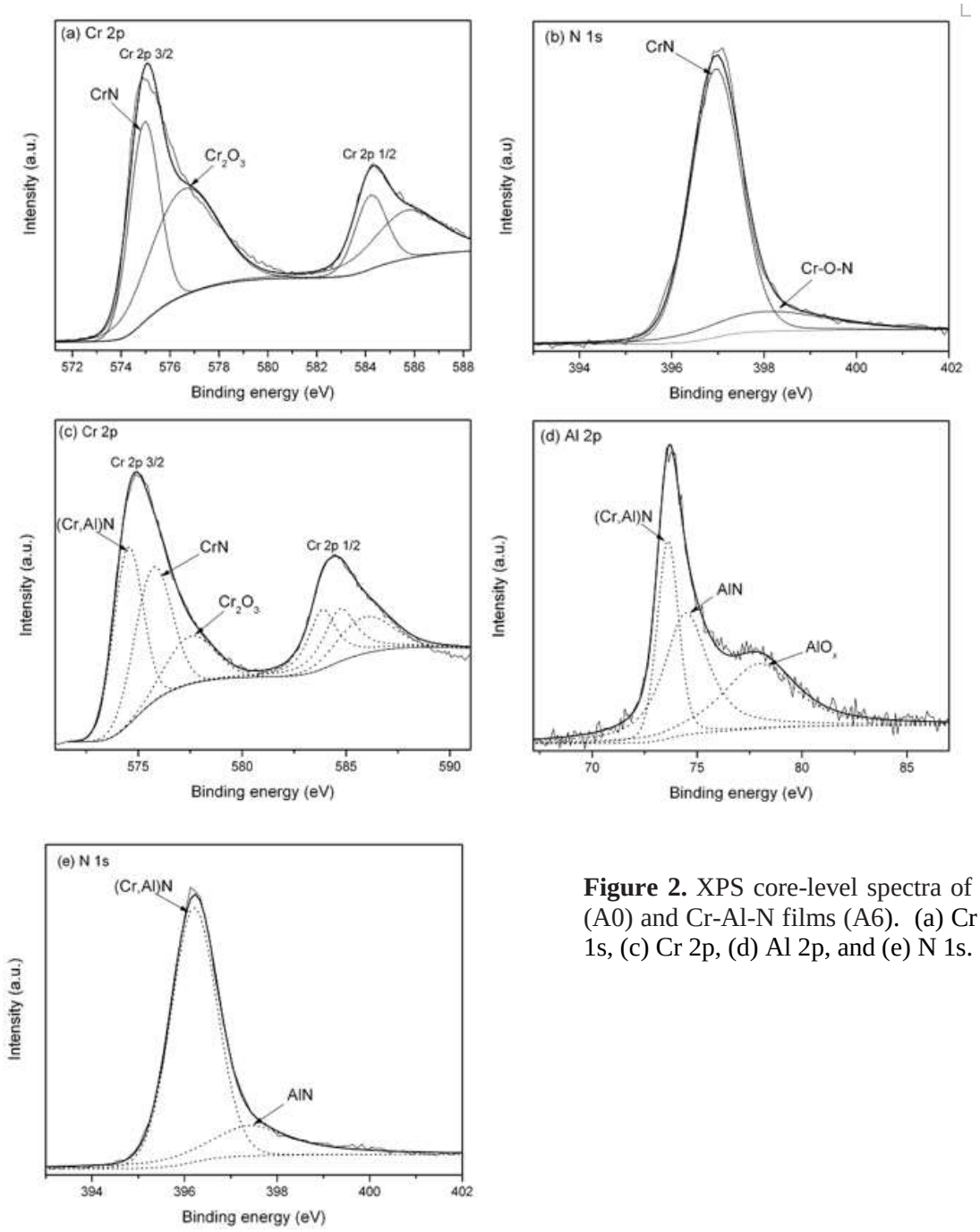

Figure 2. XPS core-level spectra of pure CrN (A0) and Cr-Al-N films (A6). (a) Cr 2p, (b) N 1s, (c) Cr 2p, (d) Al 2p, and (e) N 1s.

Such an observation was possible with TEM method as a local character of the material can be achieved when compared with XRD or XPS results. The SAED pattern in the inset of Fig. 3(b) clearly shows the diffraction rings for cubic phase nano-crystalline structure, which can be understood as solid solution of Cr(Al)N matrix embedded with few amorphous region (AlN). The film with Al content of 24.1 at.% in Fig. 3(b) shows a grown crystalline phase with grain sizes of ~11 nm, in good agreement with our XRD peak width results (calculated average grain size of ~10.8 nm).

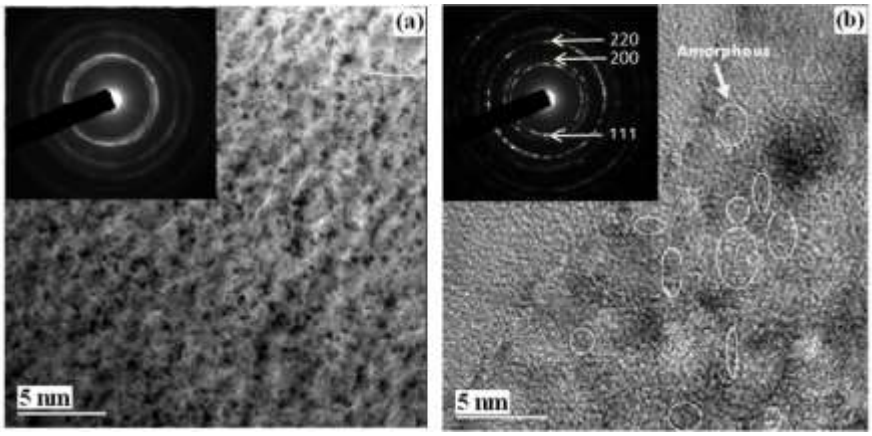

Figure 3. (a) Plane-view TEM image of pure CrN film A0 with SAED pattern in the inset; (b) HRTEM image of CrAlN film A6 with SAED pattern in the inset depicting amorphous/crystalline microstructure.

It is noted that although the Al content is only 24.1 at.%, but still promotes amorphous/crystalline microstructure. Also, to quite an extent, the amorphous/crystalline microstructure shows distinction of crystalline and amorphous phases that occur in this film. Low concentration of Al atoms will either substitute Cr atoms forming solid solution or having an interstitial substitution due to small atomic radii of Al. In addition, distinctive phase separation might be also possible with Al content of 24.1 at.% in the film.

3.3 Nanohardness

The mechanical properties of the CrAlN films were significantly affected by Al concentration. Nano-hardness and Young's modulus of the films as a function of Al content are shown in Table 1. The hardness and Young's modulus of the CrN (A0) film are 18.8 and 225 GPa, respectively. For the film A2 with 6.3 at.%, both hardness and Young's modulus values increased to 22.5 and 242 GPa. Evidently, the solid solution hardening effect contributed to the increase in the hardness of the film [27]. When the Al content was increased to 24.1 at.%, the hardness and modulus of the film further increased to maximum value of 24 GPa and 255 GPa, respectively. It is reported that the effects of solid solution hardening as well as nanocomposite interface strain strengthening mechanisms [1,2] are considered together for the hardness enhancement in the film. Increase in Al content has resulted in the decreases of the grain size too from 11.8 to 10.8 nm (based on our XRD results), consequently increasing the hardness which also suggests that high Al concentration in the film supported crystalline grain formation with less volume fraction of AlN amorphous regions. The ratio of hardness to Young's modulus *H/E* is considered as an important parameter that reflects the fracture toughness and wear properties of the films [28, 29]. The *H/E* ratio against Al content shows an analogous progression with films hardness. The film with Al content of 6.3 at.% has the highest *H/E* ratio 0.097. The hardness of A6 film is low as compared to the previously published result [30] reporting ~36 GPa (with 30 at.% of Al). In some regions, interdiffusion between the CrN and CrAlN phases could have led to comparatively a lower hardness. Previous report [26] explained that the presence of an interface energy difference between the crystallite/amorphous phase and grain boundary leads to the formation of amorphous phase which is settled at the grain boundary and can be seen in Fig. 3(a). For that reason, the mechanical properties of CrAlN films are superior than pure CrN film (A0) film, respectively.

4. Conclusions

At substrate bias voltage of -80 V and by varying target current I_{Al}/I_{Cr} ratio, a set of CrAlN films consisting ofvarious Al concentrations were successfully deposited by dc magnetron sputtering technique. All films exhibited B1 NaCl structure. The changes in the film chemistry due to the addition of Al in cubic CrN were investigated by XRD, XPS, TEM and nanoindentation tests. The

results showed that increasing target current I_{Al}/I_{Cr} ratio during deposition produced films with different Al contents, which affect the structure, phase, microstructure and hardness of the films. XRD data of CrN film showed orientation along (200) and also revealed the transition from amorphous to promotion of crystallinity in the films due to Al addition. Cr-Al-N films crystallize in cubic structure, with a preferred (200) orientation for all. The XRD results showed that fcc CrAlN films form a solid solution whereby Al atoms substitute Cr atoms. Results of XPS and TEM show clear incorporation of Al into CrN matrix resulting innanocomposite microstructure comprising of nanocrystallites and amorphous regions. The nano-hardness increased to 24 GPa with the increase in Al concentration. Maximum hardness obtained for CrAlN film is 22% superior to pure CrN film.

Acknowledgement
This work was supported by the Research Grant Council of the Hong Kong Special Administra-tive Region, China [Project No. CityU 120611 (9041679)]. YGS and ZFZ are very grateful to Dr. Y.F. Han for the contributions made in the early stages of this investigation.

References

[1] Chang YY, Chiu WT, Hung JP 2016 Surf. Coat. Technol. **303** 18.
[2] Park I W, Kang DS, Moore JJ 2007 Surf. Coat. Technol. **201** 5223.
[3] Zhang YJ, Yan PX, Wu ZG, Xu JW, Zhang WW, Li X, Liu WM, Xue QJ 2017, Tribol. Int. **115** 591.
[4] Creus J, Indriss H, Mazille H, Sanchette F, Jacquot P 1998 Surf. Coat. Technol. **107** 183-190.
[5] Gwang KS, Sang YL 2002 Surf. Coat. Technol. **171** 91.
[6] Yu C, Wang S, Tian L 2009 J Mater Sci **44** 300.
[7] Li W, Zheng KP, Liu P, Zhu PW, Zhang K, Ma FC, Liu XK, Chen XH, He DH **2016** Mat. Character. **118** 79.
[8] Martinez E, Sanjines R, Karimi A, Esteve J, L évy F 2004 Surf. Coat. Technol. **180** 570.
[9] Sabitzer C, Paulitsch J, Kolozsvari S, 2016 Thin Solid Films, **610** 26.
[10] Ding XZ, Tan ALK, Zeng XT, Wang C, Yue T, Sun CQ 2008 Thin Solid Films **516** 5716.
[11] Tillmann W**,** Stangier D**,** Schroder P 2016 Surf. Coat. Technol. **308** 147.
[12] Long Y, Zeng J, Donghai Y, Wu S 2014 Ceramics International **40** 9889.
[13] Heim D, Holler F and Mitterer C 1999 Surf. Coat. Technol. **116** 530.
[14] Beliardouh NE, Bouzid K, Nouveau C, Tlili B, Walock MJ 2014 Tribol. Inter. **82** 443.
[15] Chen X, Yeting X, Jie M, Pang X, Yang H 2016 Journal of Alloys and Compounds, **665** 210.
[16] Lin J, Mishra B, Moore JJ, Sproul WD 2006 Surf. Coat. Technol. **201** 4329.
[17] Makino Y, Nogi K 1998 Surf. Coat. Technol. **98** 1008.
[18] Sugishima A, Kajioka H, Makino Y 1997 Surf. Coat. Technol. **97** 590.
[19] Yanhong LV, Li J, Liu X, Li H, Zhou H, Chen J 2012 App. Surf. Sci. **258** 3864.
[20] Lin J, Moore JJ, Mishra B, Pinkas M, Sproul WD, Rees JA 2008 Surf. Coat. Technol. **202** 1418.
[21] Abadias G 2008 Surf. Coat. Technol. **202** 2223.
[22] Wang L, Zhang G, Wood RJK, Wang SC, Xue Q 2010 Surf. Coat. Technol. **204** 3517.
[23] Li Z, Munroe P, Jiang ZT, Zhao X, Xu J, Zhou ZF, Jiang JQ, Fang F, Xie ZH 2012 Acta Materialia **60** 5735.
[24] Emery C, Chourasia AR, Yashar P 1999 J. Electron Spectrosc. Relat. Phenom. **104** 91.
[25] Lippitz A, Hubert T 2005 Surf. Coat. Technol. **200** 250.
[26] Barshilla HC, Selvakumar N 2006 Surf. Coat. Technol. **201** 2193.
[27] Liu ZJ, Shen YG 2004 Acta Mater. **52** 729.
[28] Musil J 2000 Surf. Coat. Technol. **125** 322.
[29] Khlifi K, Dhiflaoui H, Zoghlami L 2015 J. Mater. Eng. Perfor. **24** 4077.
[30] Tlili B, Mustapha N, Nouveau C, Benlatreche Y, Guillemot G, Lambertin M 2010 Vacuum **84** 1067.